

See discussions, stats, and author profiles for this publication at: <https://www.researchgate.net/publication/263331492>

Cysteine–Cystine Redox Cycling in a Gold–Gold Dual-Plate Generator–Collector Microtrench Sensor

ARTICLE in ANALYTICAL CHEMISTRY · JUNE 2014

Impact Factor: 5.64 · DOI: 10.1021/ac501321e

CITATIONS

6

READS

98

9 AUTHORS, INCLUDING:



Andrew J Gross

University Joseph Fourier - Grenoble 1

22 PUBLICATIONS 121 CITATIONS

[SEE PROFILE](#)



Pedro Estrela

University of Bath

90 PUBLICATIONS 788 CITATIONS

[SEE PROFILE](#)



Charles Peter Winlove

University of Exeter

169 PUBLICATIONS 2,505 CITATIONS

[SEE PROFILE](#)



Paul Graham Winyard

University of Exeter

198 PUBLICATIONS 5,378 CITATIONS

[SEE PROFILE](#)

¹ Cysteine-Cystine Redox Cycling in a Gold–Gold Dual-Plate Generator-Collector Microtrench Sensor

³ Jules L. Hammond,[†] Andrew J. Gross,[‡] Pedro Estrela,[†] Jesus Iniesta,[§] Stephen J. Green,^{||}
⁴ C. Peter Winlove,^{||} Paul G. Winyard,[⊥] Nigel Benjamin,[⊥] and Frank Marken*,^{†‡}

⁵ [†]Department of Electronic & Electrical Engineering, University of Bath, Bath BA2 7AY, U.K.

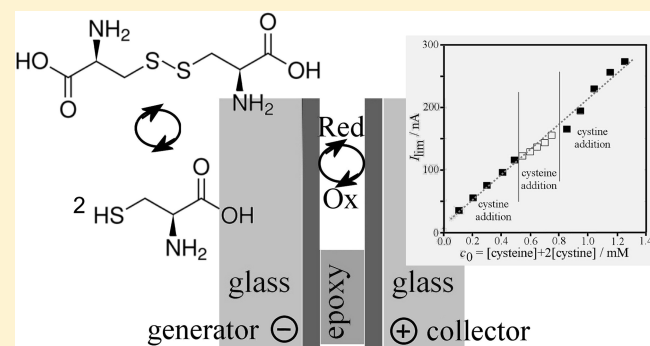
⁶ [‡]Department of Chemistry, University of Bath, Bath BA2 7AY U.K.

⁷ Universidad Alicante, Department of Physical Chemistry and Institute for Electrochemistry, 03080 Alicante, Spain

⁸ ^{||}Department of Physics, College of Engineering, Mathematics and Physical Sciences, University of Exeter, Stocker Road, Exeter EX4 4QL, U.K.

¹⁰ [⊥]University of Exeter Medical School, University of Exeter, St. Luke's Campus, Exeter, EX1 2LU, U.K.

ABSTRACT: Thiols and disulfides are ubiquitous and important analytical targets. However, their redox properties, in particular on gold sensor electrodes, are complex and obscured by strong adsorption. Here, a gold–gold dual-plate microtrench dual-electrode sensor with feedback signal amplification is demonstrated to give well-defined (but kinetically limited) steady-state voltammetric current responses for the cysteine-cystine redox cycle in nondegassed aqueous buffer media at pH 7 down to micromolar concentration levels.



Cysteine is an α -amino acid found in many natural proteins and physiological media. Cystine, the oxidized dimer of cysteine, provides a modality for the cross-linking through disulfide bonds, important in defining the primary, secondary, and tertiary structure of proteins. The sulfhydryl group in cysteine is partially deprotonated at physiological pH, enhancing reactivity and allowing the formation of reversible oxidative post-translational modifications (oxPTMs) that act as a signaling mechanism, regulating protein function, interaction, and localization.^{1,2} *In vivo*, thiol–disulfide redox cycling is catalyzed by thiol oxidases and disulfide reductases in the endoplasmic reticulum and periplasmic space.³ Typical concentrations of L-cysteine in blood plasma are between 200 and 300 μ M and can be useful as a medical indicator in human diseases involving abnormal cysteine metabolism.⁴

The electrochemical detection of the cysteine-cystine redox couple offers the advantages of being more affordable and miniaturizable as well as providing fast and sensitive detection when compared to spectrometric⁵ or chromatography⁶ techniques. However, in particular for thiols and disulfides, very few analytical procedures have been developed due to the complexity of these redox systems. The oxidation of cysteine has been investigated on different types of electrodes^{7–9} and found to proceed (depending on electrode material and applied potential) via multielectron pathway producing cysteic acid (six electrons) as final product with further complications due to strong thiol adsorption on metal surfaces. The one-electron product, cystine, also is strongly adsorbed and requires highly

negative applied potential for reductive desorption back to cysteine.¹⁰ A new method to overcome this chemical complexity can be based on generator-collector sensors.¹¹

Advantages of amplification by generator-collector feedback have been pioneered and exploited for example by Christensen,¹² by Hubbard,¹³ and by Seddon.¹⁴ More recently Lemay has demonstrated nanoscale generator-collector electrode systems with extreme sensitivity down to the single molecule level.^{15–17} Pulse methods were reported for glucose detection in a gold–gold dual-hemisphere electrode system with a nanogap.¹⁸ Microtrench or dual-plate electrodes with an interelectrode gap of typically 2–80 μ m and an aspect ratio of typically 10 have been developed to allow, for example, dopamine detection,¹⁹ pH titration,²⁰ and liquid–liquid anion transfer detection.²¹ The benefits of this dual-plate electrode geometry are (i) rapid and mostly planar interelectrode diffusion within the trench, (ii) rapid diffusion of analyte into the trench, (iii) discrimination of chemically reversible targets from irreversible interferences (e.g., oxygen or ascorbate), and (iv) improved specificity from two applied electrode potentials. In this report a gold–gold dual-plate microtrench sensor is employed for the detection of cysteine-cystine.

Received: April 11, 2014

Accepted: June 17, 2014

71 Figure 1A shows a schematic depiction of the simplified
72 reaction scheme with the redox system cysteine-cystine

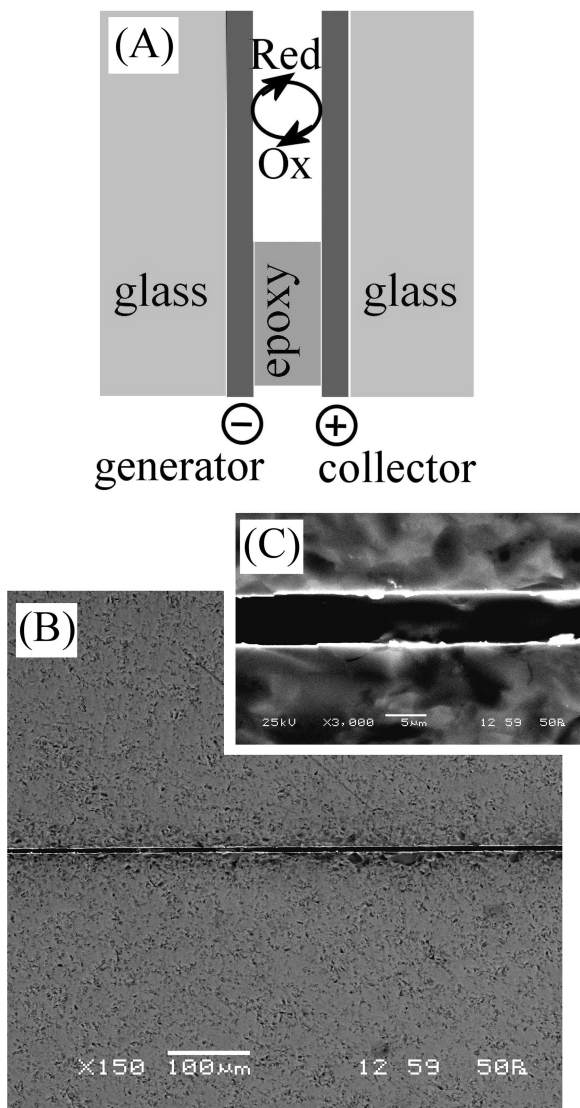


Figure 1. (A) Schematic drawing of the microtrench sensor in feedback mode. (B,C) SEM images of the gold–gold dual-plate microtrench with $\sim 6 \mu\text{m}$ width.

73 represented by Red/Ox. The gold–gold dual-plate microtrench
74 electrode employed here should allow steady state current
75 responses to be obtained irrespective of the complexity in the
76 reaction scheme and with potential for future analytical
77 applications.

78 ■ EXPERIMENTAL SECTION

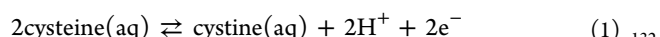
79 **Reagents.** L-cysteine (97%), L-cystine (99%), sodium
80 hydroxide (98–100.5%), sodium phosphate monobasic (98–
81 102%), and potassium chloride (99–100.5%) were purchased
82 from Sigma-Aldrich and used without further purification.
83 Purified water (18.2 MΩ cm) from a PURELAB Classic purifier
84 (ELGA) was used to make solutions. L-cysteine was stored below
85 5 °C and both L-cysteine and L-cystine solutions were prepared
86 immediately before use with 1 min sonication to assist
87 solubilization.

Instrumentation. Electrochemical measurements were 88 performed using an Autolab PGSTAT12 (Metrohm) bipotentio- 89 stat equipped with a differential electrometer amplifier. A four- 90 electrode arrangement was utilized, composed of a saturated KCl 91 calomel electrode (SCE, Radiometer REF 401), platinum wire 92 counter electrode, and the two working electrodes of the gold– 93 gold microtrench electrode. In some experiments, a conventional 94 1 mm diameter gold disc working electrode was employed in a 95 three-electrode arrangement. A Teflon jig was used to hold the 96 four electrodes in place within a 50 mL glass beaker. GPES 97 software was used to perform cyclic voltammetry at the generator 98 while holding the collector electrode at a constant voltage. Linear 99 baseline correction within GPES was used to improve 100 presentation of data where appropriate. SEM images were 101 taken with a SEM6480LV microscope (JEOL). 102

Procedure: Growth of Gold–Gold Junction Electrodes. 103 Figure 1B,C shows SEM images of the microtrench electrode 104 with $\sim 6 \mu\text{m}$ interelectrode gap. This type of electrode has a depth 105 of $\sim 60 \mu\text{m}$ (aspect ratio 10; determined by electrochemical 106 calibration with a $\text{Fe}(\text{CN})_6^{3-/4-}$ redox system²⁰). The fabrication 107 was based on 100 nm gold-coated microscope slides (Sigma- 108 Aldrich), which were sliced into 10 mm \times 25 mm strips using a 109 diamond cutter (Buehler Isomet 1000). A central 5 mm \times 25 mm 110 region of a strip was masked using Kapton tape before etching the 111 exposed gold for 3 min using aqua regia (1:3 nitric acid– 112 hydrochloric acid; warning: this solution is highly corrosive). The 113 etching process was stopped by rinsing with water. In order to 114 oxidize the remaining titanium adhesion layer, the electrodes 115 were placed into a furnace at 500 °C for 30 min. Epoxy (Gurit 116 SP106) was used to bond two opposing electrodes, with the 117 epoxy given 1 h to cure before application of pressure. The 118 base of the microtrench was sliced off using a diamond cutter and 119 polished using decreasing grits of SiC abrasive paper (Buehler). 120 Finally, the epoxy was etched out using piranha solution (5:1 121 sulfuric acid–hydrogen peroxide; warning: this solution is highly 122 corrosive) to form the trench. 123

■ RESULTS AND DISCUSSION

Cysteine-Cystine Redox Processes at Gold Electrodes. 125 The oxidation of cysteine is known to occur in a complex 126 multielectron process via cystine to give products including 127 cysteic acid,^{22,23} in particular, in alkaline media. However, when 128 performed under controlled potential conditions and at neutral 129 pH, the one-electron oxidation per cysteine to cystine should be 130 observed (eq 1). 131



On gold electrodes further processes are expected due to 133 effective adsorption of thiols and disulfides to the surface and due 134 to the well-known gold surface oxidation in aqueous phosphate 135 buffer at pH 7.²⁴ Figure 2A shows typical cyclic voltammograms 136 f2 with (i) a background response consistent with gold and (ii) a 137 clear oxidation peak at 0.6 V vs SCE similar for example to that 138 reported for N-acetyl-cysteine.²⁵ The peak current of $\sim 22 \mu\text{A}$ 139 allows the apparent diffusion coefficient for cysteine to be 140 estimated based on the Randles–Sevcik equation, which is 141 employed here only to provide an approximate bench mark value 142 for the diffusion limited peak current (eq 2). 143

$$I_p = 0.446 \times nFAC \sqrt{\frac{nFvD}{RT}} \quad (2) \quad 144$$

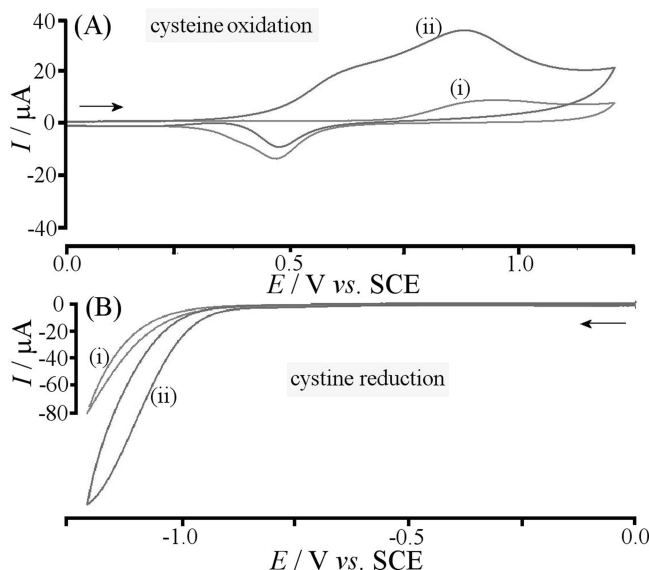


Figure 2. Cyclic voltammograms (scan rate 0.1 V s^{-1} , 1 mm diameter gold disc electrode, 0.1 M phosphate buffer pH 7) for (A) the oxidation of 1 mM cysteine and (B) the reduction of 1 mM cysteine. The trace (i) shows the background signal without analyte.

In this equation, I_p is the peak current, $n = 1$ is assumed for cysteine formation (*vide infra*), F is the Faraday constant, v is the potential scan rate, R is the gas constant, T is the absolute temperature, and the apparent diffusion coefficient D can then be obtained as $6 \times 10^{-9} \text{ m}^2 \text{ s}^{-1}$. This value is much too high to be physically realistic (the literature value is $D_{\text{cysteine}} = 0.81 \times 10^{-9} \text{ m}^2 \text{ s}^{-1}$)²⁶ and therefore an indication of either (i) multielectron transfer, or (ii) contributions from adsorbed cysteine, or both. It is known that cysteine strongly adsorbs onto gold electrode prior to oxidation.²⁷

The back-reduction of cystine to cysteine formally is a 2-electron process (see eq 1) and has been reported previously, for example, on Pb electrodes.²⁸ The diffusion coefficient was determined as $D_{\text{cystine}} = 0.48 \times 10^{-9} \text{ m}^2 \text{ s}^{-1}$. Data in Figure 2B suggest that there is a cystine reduction at the gold electrode surface commencing at -0.8 V vs SCE but without clear peak feature and with a quite high current ($\sim 40 \mu\text{A}$ at -1.2 V vs SCE), therefore again affected by adsorption of cystine on the electrode. In addition to the reduction response for cystine, an oxidation response similar to that observed for cysteine at 0.6 V vs SCE (not shown) is observed, indicative of more complexity involving surface-adsorbed intermediates and/or multielectron oxidation or cystine to cysteic acid. Given the complexity observed for cysteine-cystine at single gold electrodes, it is interesting to explore reactivity at the Au–Au dual-plate generator-collector electrode systems. The observation of a cysteine-cystine redox cycle would offer a way to distinguish the well-defined redox cycle from more complex redox and background processes.

Generator-Collector Processes I: Oxidation of Cysteine. Initial experiments at the Au–Au generator-collector microtrench electrode were performed with the generator scanning into the cysteine oxidation and the collector at fixed potential. Figure 3A shows that there was indeed a feedback current with the collector potential held sufficiently negative, here -0.5 V vs SCE , with good responses being recorded at $E_{\text{collector}} = -0.85 \text{ V vs SCE}$. Next, the cysteine concentration was varied (see Figure 3B) and the plot of collector current versus concentration shows reasonable linearity, consistent with a

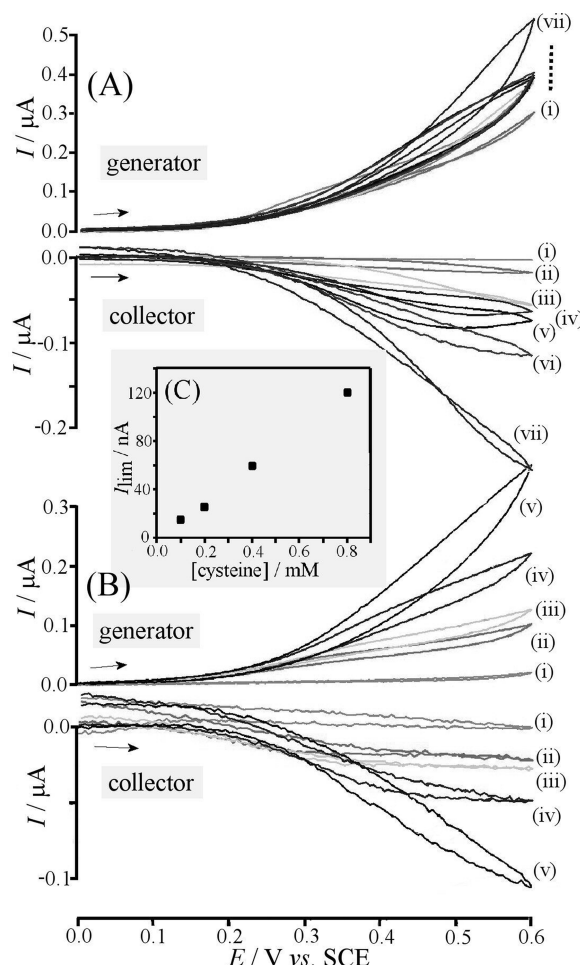


Figure 3. Generator-collector voltammograms (scan rate 0.025 V s^{-1} , gold–gold dual-plate microtrench, 0.1 M phosphate buffer pH 7) for the oxidation and back-reduction of 1 mM cysteine. (A) Data obtained with collector potentials (i) -0.25 , (ii) -0.45 , (iii) -0.55 , (iv) -0.65 , (v) -0.75 , (vi) -0.85 , (vii) -0.95 V vs SCE . (B) Data obtained with collector potential -0.85 and (i) 0, (ii) 0.1, (iii) 0.2, (iv) 0.4, (v) 0.8 mM cysteine. (C) Plot of limiting current versus concentration of cysteine.

generator-collector feedback process (see Figure 3C). In spite of the complexity of the overall redox process, a feedback current can be identified tentatively (assuming mass transport control) expressed in terms of the Nernst model for dual-plate diffusion processes²⁰ as

$$I_{\text{lim,diffusion}} = \frac{2FAc_0}{\delta} \frac{D_{\text{cysteine}} \times D_{\text{cystine}}}{D_{\text{cysteine}} + D_{\text{cystine}}} \quad (3)$$

In this equation, $I_{\text{lim,diffusion}}$ is the microtrench feedback current under mass transport control, F and A are the Faraday constant and electrode area, $\delta = 6 \mu\text{m}$ is the interelectrode gap, and the concentration is defined as $c_0 = 2c_{\text{cystine}} + c_{\text{cysteine}}$. On the basis of this expression, and with a $60 \mu\text{m}$ trench depth, the predicted slope for the plot in Figure 3C is $2.9 \mu\text{A mM}^{-1}$, which is 20 times higher than that observed experimentally. Therefore, the feedback current appears to be inconsistent with diffusion control and more likely to be kinetically limited (*vide infra*).

Generator-Collector Processes II: Reduction of Cystine. The cystine reduction at the Au–Au microtrench is mechanistically equivalent to the case of cysteine oxidation (the same coupled redox chemistry occurs with generator and collector

switching roles, see eq 1). Voltammetric data in Figure 4A show the onset of the collector response with the collector potential set

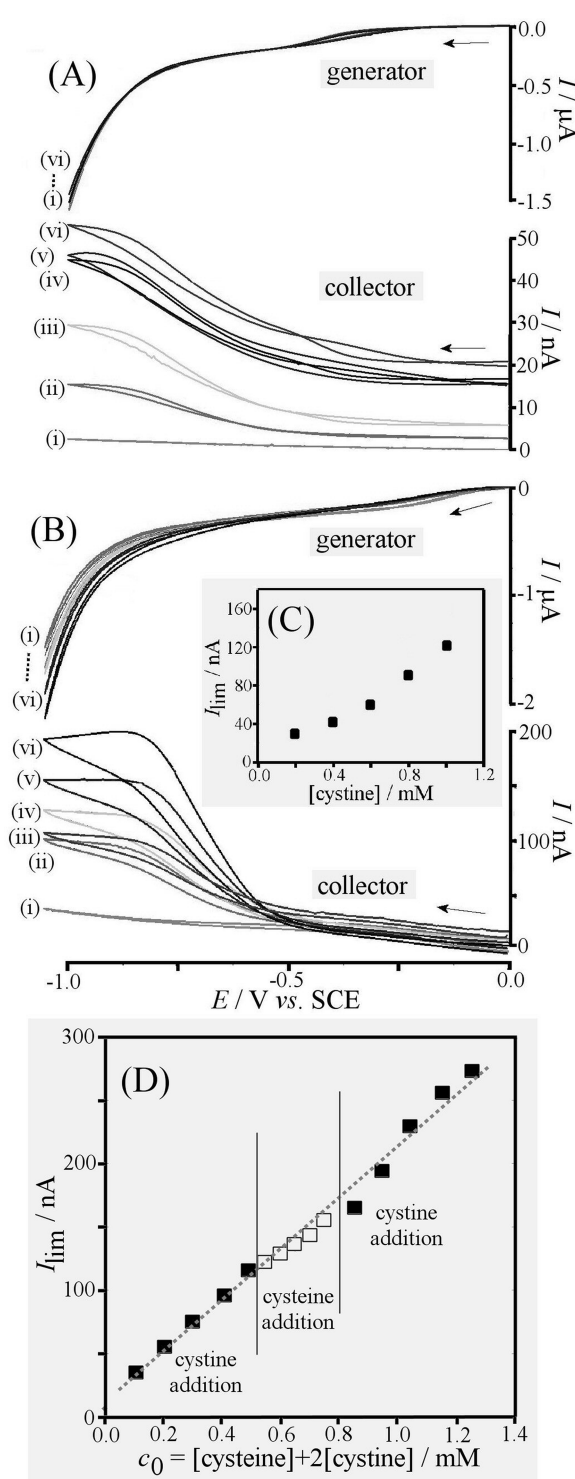


Figure 4. Generator-collector voltammograms (scan rate 0.025 V s^{-1} , gold–gold dual-plate microtrench, 0.1 M phosphate buffer pH 7) for the reduction and back-oxidation of 1 mM cystine. (A) Data obtained with collector potentials (i) 0.15 , (ii) 0.35 , (iii) 0.55 , (iv) 0.60 , (v) 0.65 , (vi) 0.70 V vs SCE (data shifted along current axis to overlay). (B) Data obtained with collector potential 0.60 and (i) 0 , (ii) 0.2 , (iii) 0.4 , (iv) 0.6 , (v) 0.8 , (vi) 1.0 mM cystine. (C) Plot of limiting current versus concentration of cystine. (D) Plot for limiting current versus c_0 for sequential $50 \mu\text{M}$ addition of both cysteine and cystine.

to 0.4 V vs SCE with good feedback currents observed with collector potential 0.6 V vs SCE. An offset current in the collector response is indicative of some additional oxidation (possibly multielectron thiol oxidation) at this potential. A current step in the generator signal at -0.4 V vs SCE shows a weak oxygen reduction (solutions were not deaerated) without significant effect on the collector response.

When varying the cystine concentration (with 0.6 V vs SCE collector potential), a well-defined feedback current is detected at -0.8 V vs SCE generator potential (Figure 4B) and a plot of the observed current versus cystine concentration (Figure 4C) suggests approximately linear correlation. The current–concentration slope observed experimentally is again an order of magnitude lower than that expected based on eq 3. Therefore, simple diffusion controlled reaction conditions are unlikely to govern this process. It is possible to express the case of a kinetically limited microtrench process based on $I_{\text{ox}} = FAK_{\text{ox}} [\text{cysteine}]$ and $I_{\text{red}} = 2FAk_{\text{red}} [\text{cystine}]$. Irrespective of the nature of k_{ox} and k_{red} equating these two expressions shows that $[\text{cystine}]/[\text{cysteine}] = k_{\text{ox}}/2k_{\text{red}}$, which suggests that depending on the applied potential either cystine or cysteine will be present in the microtrench. Substitution with $c_0 = [\text{cysteine}] + 2[\text{cystine}]$ then gives the microtrench limiting current as

$$I_{\text{lim,kinetic}} = FAc_0 \frac{k_{\text{ox}} \times k_{\text{red}}}{k_{\text{ox}} + k_{\text{red}}} \quad (4)$$

A kinetically controlled limiting current should be obtained linear in c_0 . This is demonstrated in Figure 4D for sequential $50 \mu\text{M}$ additions of cystine and cysteine. The agreement with eq 4 is acceptable and remaining nonlinearity may be associated with the adsorption/desorption kinetics, some degree of multi-electron oxidation, and the transient nature of the cyclic voltammetry experiment. Effects of adsorption kinetics, in particular in nanogap sensors, have been discussed recently by Mathwig and Lemay.²⁹

It is interesting to note that all experiments here were conducted in the presence of ambient levels of oxygen. The reduction of oxygen is observed at the generator at -0.4 V vs SCE (see Figure 4A), but this appears not to interfere with the cysteine-cystine redox signal. For the overall cysteine-cystine process there are two possible scenarios to explain the lower than diffusion-limited current responses: (A) If the cysteine oxidation occurs as a multielectron process with products other than cystine, this will induce a concentration depletion effect within the microtrench. (B) If a slow surface process is associated with a kinetically limiting factor (most likely slow electron transfer associated with adsorption/desorption), lower conversion and therefore lower currents would be expected during feedback across the microtrench.

The second hypothesis appears to be most likely here, but the first process may also contribute significantly. In the future, further experiments are required with either a mesoporous gold electrode surface (to overcome slow surface processes with high surface area³⁰) or a significantly smaller interelectrode gap (to overcome/outrun multielectron transfer depletion effects). Other electrode materials and/or electrocatalysts could be introduced to provide “fingerprint” information on different types of thiols and disulfides.

CONCLUSION

It has been demonstrated that even for complex analytical systems such as cysteine-cystine on gold at pH 7 and in the

263 presence of air, dual-plate generator-collector electrode systems
 264 allow analytically useful current responses to be obtained.
 265 Interfering current signals such as those from gold surface
 266 oxidation and/or thiol adsorption are suppressed and the
 267 analytical signal of interest is feedback-enhanced. For both
 268 processes, cysteine oxidation and cystine reduction, similar
 269 behavior and similar sensitivity were observed in accordance with
 270 the equivalence of both in the overall microtrench redox cycle. It
 271 is likely that some anodic overoxidation of cysteine is a factor
 272 here in suppressing the analytical signal due to depletion of
 273 analyte within the microtrench. Even more important is probably
 274 the kinetic limitation inherent in cysteine oxidation and in cystine
 275 reduction when adsorbed on gold. In the future, submicrometer
 276 "nano-trench" electrode systems based on appropriate or better
 277 electrode materials may allow short-lived intermediates such as
 278 the cysteine radical to be "caught" and redox-recycled more
 279 effectively. Sensing applications are feasible for a wider range of
 280 thiols and under physiological conditions.

281 ■ AUTHOR INFORMATION

282 Corresponding Author

283 *E-mail: F.Marken@bath.ac.uk.

284 Notes

285 The authors declare no competing financial interest.

286 ■ ACKNOWLEDGMENTS

287 J.L.H. is supported by an U.K. Engineering and Physical Sciences
 288 Research Council (EPSRC) Doctoral Training Award. A.J.G. and
 289 F.M. gratefully acknowledge EPSRC funding (Grant EP/
 290 I028706/1).

291 ■ REFERENCES

- 292 (1) Paulsen, C.; Carroll, K. *Chem. Rev.* **2013**, *113*, 4633–4679.
- 293 (2) Winyard, P. G.; Moody, C. J.; Jacob, C. *Trends Biochem. Sci.* **2005**,
 294 *30*, 453–461.
- 295 (3) Sevier, C.; Kaiser, C. *Nat. Rev. Mol. Cell Biol.* **2002**, *3*, 836–847.
- 296 (4) Salemi, G.; Gueli, M.; D'Amelio, M.; Saia, V.; Mangiapane, P.;
 297 Aridon, P.; Ragonese, P.; Lupo, I. *Neurol. Sci.* **2009**, *30*, 361–364.
- 298 (5) Hao, W. H.; McBride, A.; McBride, S.; Gao, J. P.; Wang, Z. Y. *J. Mater. Chem.* **2011**, *21*, 1040–1048.
- 299 (6) Guan, X.; Hoffman, B.; Dwivedi, C.; Matthees, D. P. *J. Pharm. Biomed. Anal.* **2003**, *31*, 251–261.
- 300 (7) Ralph, T. R.; Hitchman, M. L.; Millington, J. P.; Walsh, F. C. *J. Electroanal. Chem.* **1994**, *375*, 1–15.
- 301 (8) Lai, Y. T.; Ganguly, A.; Chen, L. C.; Chen, K. H. *Biosens. Bioelectron.*
 302 **2010**, *26*, 1688–1691.
- 303 (9) Shaidarova, L. G.; Ziganshina, S. A.; Gedmina, A. V.; Chelnokova, I.
 304 A.; Budnikov, G. K. *J. Anal. Chem.* **2011**, *66*, 633–641.
- 305 (10) Wang, C. Y.; Liu, Q. X.; Shao, X. Q.; Hu, X. Y. *Anal. Lett.* **2007**, *40*,
 306 689–704.
- 307 (11) Barnes, E. O.; Lewis, G. E. M.; Dale, S. E. C.; Marken, F.;
 308 Compton, R. G. *Analyst* **2012**, *137*, 1068–1081.
- 309 (12) Christensen, C. R.; Anson, F. C. *Anal. Chem.* **1963**, *35*, 205–209.
- 310 (13) Hubbard, A. T.; Peters, D. G. *CRC Crit. Rev. Anal. Chem.* **1973**, *3*,
 311 201–242.
- 312 (14) Seddon, B. J.; Wang, C. F.; Peng, W. F.; Zhang, X. J. *J. Chem. Soc., Faraday Trans.* **1994**, *90*, 605–608.
- 313 (15) Katelhon, E.; Hofmann, B.; Lemay, S. G.; Zevenbergen, M. A. G.;
 314 Offenhausser, A.; Wolfrum, B. *Anal. Chem.* **2010**, *82*, 8502–8509.
- 315 (16) Zevenbergen, M. A. G.; Singh, P. S.; Goluch, E. D.; Wolfrum, B.
 316 L.; Lemay, S. G. *Nano Lett.* **2011**, *11*, 2881–2886.
- 317 (17) Kang, S.; Nieuwenhuis, A.; Mathwig, K.; Mampallil, D.; Lemay, S.
 318 G. *ACS Nano* **2013**, *7*, 10931–10937.
- 319 (18) Rassaei, L.; Marken, F. *Anal. Chem.* **2010**, *82*, 7063–7067.
- 320 (19) Hasnat, M. A.; Gross, A. J.; Dale, S. E. C.; Barnes, E. O.; Compton, R. G.; Marken, F. *Analyst* **2013**, *139*, 569–575.
- 321 (20) Dale, S. E. C.; Vuorema, A.; Sillanpää, M.; Weber, J.; Wain, A. J.; Barnes, E. O.; Compton, R. G.; Marken, F. *Electrochim. Acta* **2014**, *125*, 94–100.
- 322 (21) Dale, S. E. C.; Chan, Y.; Bulman Page, P. C.; Barnes, E. O.; Compton, R. G.; Marken, F. *Electrophoresis* **2013**, *34*, 1979–1984.
- 323 (22) Sires, I.; Delucchi, M.; Panizza, M.; Ricotti, R.; Cerisola, G. *J. Appl. Electrochim. *2009**, *39*, 2275–2284.
- 324 (23) Enache, T. A.; Oliveira-Brett, A. M. *Bioelectrochemistry* **2011**, *81*, 46–52.
- 325 (24) Milsom, E. V.; Novak, J.; Oyama, M.; Marken, F. *Electrochim. Commun.* **2007**, *9*, 436–442.
- 326 (25) Barus, C.; Gros, P.; Comtat, M.; Daunes-Marion, S.; Tarroux, R. *Electrochim. Acta* **2007**, *52*, 7978–7985.
- 327 (26) Abbaspour, A.; Ghaffarinejad, A. *Electrochim. Acta* **2008**, *53*, 6643–6650.
- 328 (27) Uvdal, K.; Bodo, P.; Liedberg, B. *J. Colloid Interface Sci.* **1992**, *149*, 162–173.
- 329 (28) Ralph, T. R.; Hitchman, M. L.; Millington, J. P.; Walsh, F. C. *J. Electroanal. Chem.* **2005**, *583*, 260–272.
- 330 (29) Mathwig, K.; Lemay, S. G. *Electrochim. Acta* **2013**, *112*, 943–949.
- 331 (30) Liu, Z.; Zhang, H. C.; Hou, S. F.; Ma, H. *Microchim. Acta* **2012**, *177*, 427–433.